THE JOURNAL OF PHYSICAL CHEMISTRY C
A JOURNAL OF THE AMERICAN CHEMICAL SOCIETY

pubs.acs.org/JPCC

Article

Arylazo under Extreme Conditions: [2 + 2] Cycloaddition and Azo Metathesis

Dexiang Gao,[○] Xingyu Tang,[○] Chunfang Zhang, Yajie Wang, Xin Yang, Peijie Zhang, Xuan Wang, Jingqin Xu, Jie Su, Fuyang Liu, Xiao Dong, Xiaohuan Lin, Bao Yuan, Nozomu Hiraoka, Haiyan Zheng,* Le Kang,* Kuo Li, and Ho-kwang Mao

Cite This: *J. Phys. Chem. C* 2023, 127, 8482−8492

Read Online

ACCESS | Metrics & More | Article Recommendations | Supporting Information

ABSTRACT: The four-membered nitrogen ring (N_4-ring) is predicted to be a high-energy density moiety and has been the target of chemical synthesis for quite a long time. Here, by compressing the 1:1 co-crystal of *trans*-azobenzene and *trans*-perfluoroazobenzene up to ~40 GPa, the azo groups were restrained closely in parallel in the crystal and underwent two competitive addition reactions. One is [4 + 2] cycloaddition with the azo group as a part of diene and phenyl as dienophile. The other is [2 + 2] cycloaddition between two azo groups, which produced an unprecedented N_4-ring structure as evidenced by the metathesis product. The content of the N_4-ring structure significantly increases under higher pressure, and we found that it was the external pressure that decreased the kinetic barrier and realized such a high-tensile moiety. Our work shows that high pressure is an alternative synthetic strategy for these high-tensile structures, which can be very effective under the cooperation of crystal engineering.

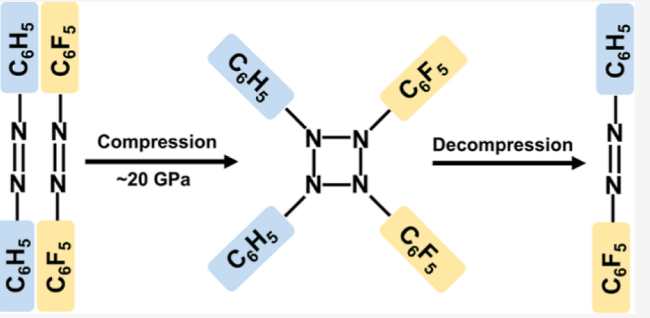

INTRODUCTION

Polynitrogen compounds are important high energy density materials because they can release a huge amount of energy when N−N and N═N bonds (bond energy 167 and 418 kJ/mol) transform into N≡N (942 kJ/mol).[1] Theoretically, a variety of polynitrogen structures were predicted, like N_4, N_5, N_6, and N_8 molecules with chain,[2−4] tetrahedron,[5−7] ring, and cube structures.[8−14] Experimentally, only those with extended π bonds like N_3^- and N_5 species were synthesized in an operatable scale, including the N_5^+ chain in $N_5^+AsF_6^-$ and $N_5^+SbF_6^-$, and the cyclo-N_5^- in $(N_5)_6(H_3O)_3(NH_4)_4Cl$.[15−19] Among these structures, the N_4-ring has higher energy density than others due to its higher tension and non-aromatic electron configuration and hence becomes a featured moiety focused by synthetic chemists. A cyclo-N_4 molecule was theoretically predicted with an energy of 11 kJ/mol higher than the N_4-tetrahedron, which brings a great challenge for synthesis.[20−23]

The [2 + 2] cycloaddition reaction is always a direct way to synthesize four-membered rings,[24,25] through which a series of four-membered rings like cyclobutane (C_4), azetidine (C_3N), oxetane (C_3O), thietane (C_3S), dioxetane (C_2O_2), and so forth were produced.[26−31] However, when more nitrogen atoms are introduced, the four-membered ring becomes unstable. For example, the diazetidine (C_2N_2) obtained by [2 + 2] photocycloaddition between N═N and C═C is prone to undergo the metathesis reaction and generate two C═N groups after heating.[32] By irradiating *syn*-bisdiazene, Exner et al. tried to synthesize the tetrazetidine (N_4) through the [2 + 2] cycloaddition reaction between N═N bonds, but failed due to the elimination of N_2.[33,34] Camp et al. also reported the formation of four-membered nitrogen ring by radical cyclization, but only with the evidence from electron paramagnetic resonance (ESR) spectroscopy.[35] Up to now, all attempts to induce the cycloadditions between two N═N are unsuccessful, even the metathesis product was not observed, and whether tetrazetidine (N_4) can exist (even in the metastable state) is still controversial.

High pressure is a promising method to synthesize N_4-ring. First, external pressure can greatly compress the intermolecular N···N distance and induce the N−N bonding, like in the synthesis of cubic gauche polymeric nitrogen under 110 GPa with three-connected N atoms and 10-membered rings, layered polymeric nitrogen above 120 GPa with single-bonded 7-membered ring structure, and singly bonded amorphous nitrogen under 150 GPa.[36−38] Second, external pressure usually

Received: March 2, 2023
Revised: April 11, 2023
Published: April 26, 2023

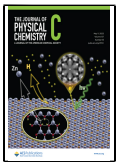

https://doi.org/10.1021/acs.jpcc.3c01450
J. Phys. Chem. C 2023, 127, 8482−8492

suppresses the production of gas,[39,40] which would help to avoid the elimination of N_2. In this work, aiming at the N═N addition reaction, we prepared the co-crystal of azobenzene (AB) and perfluoroazobenzene (FAB), in which the strong intermolecular interaction guarantees the closed parallel stacking of the molecules and the azo groups. We found under high pressure AB−FAB experienced an unexpected Diels−Alder addition reaction between aryl−azo (diene) and aryl (dienophile), completely different with the reactions of azo at ambient pressure. More importantly, we also found the azo metathesis between AB and FAB via a N_4-ring intermediate, providing a potential route to synthesize a N_4-ring moiety. Our work clearly reveals the characteristics of the addition reaction on −N═N−, especially the reaction selectivity under high pressure, which has great inspiration for the synthesis of covalent-bonded nitrogen materials.

MATERIALS AND METHODS

Preparation of Co-crystal *trans*-Azobenzene and *trans*-Perfluoroazobenzene and Its Characterization. The powder azobenzene (AB, 98%) was recrystallized in *n*-hexane and the *trans*-perfluoroazobenzene was synthesized according to the method reported in the literature (the experimental procedure and its characterization shown in Supporting Information).[41] The single crystal of 1:1 co-crystal of *trans*-azobenzene (AB) and *trans*-perfluoroazobenzene (FAB) were prepared by slow evaporation of the AB and FAB mixture in *n*-hexane. The sample was identified as 1:1 co-crystal without impurity in single crystal X-ray diffraction (XRD) experiment at 180 K on a Rigaku XtaLAB PRO 007HF(Mo) diffractometer, with Mo K_α radiation (λ = 0.71073 Å). The CrysAlisPro program was used to perform the data reduction and empirical absorption correction. The structure was solved by a dual-space algorithm using SHELXT program.[42] All non-hydrogen atoms could be located directly from the difference Fourier maps. Framework hydrogen atoms were placed geometrically and constrained using the riding model to the parent atoms. Final structure refinement was done using the SHELXL program by minimizing the sum of squared deviations of F2 using a full-matrix technique.

In Situ Raman, IR, Inelastic X-ray Raman, and X-ray Diffraction under High Pressure. The obtained 1:1 co-crystal, AB−FAB, was used for in situ Raman, IR, and X-ray Raman spectrum (XRS) measurements. In the in situ Raman and IR experiments, symmetrical diamond anvil cell (DAC) with 300 μm culet was used for applying pressure. T-301 stainless steel gaskets were pre-indented to a thickness of 35 μm and holes of 120 μm in diameter were drilled in the center of the indentation to serve as the sample chamber. In situ Raman spectra were recorded on a Renishaw Raman microscope with excitation laser wavelength at 532 nm. For in situ IR experiments, a pair of type II diamonds was used, and a disk of dried KBr powder with appropriate size and thickness was filled into the sample chamber to reduce the thickness of the sample. The data were collected in the transmission mode on the Bruker VERTEX 70v spectrometer with HYPERION 2000 microscope and Globar source. The collection range was 600−4000 cm^{-1} with a resolution of 2 cm^{-1}. No pressure media was used and the ruby fluorescence was used to calibrate the pressure when performing the in situ Raman and IR measurements.[43] Inelastic XRS was collected on BL12XU of Spring-8. Beryllium gasket and symmetrical DAC were used in in situ X-ray Raman experiments. At a scattering angle of 30°, the Si (555) analyzer with a fixed elastic energy (E_0) of 9.886 KeV was used to refocus scattered X-ray photons onto the detector by using the back scattering geometry methods.[44] For N edge measurement, the energy of incident X-ray was scanned from 10316 to 10266 eV. For C edge measurement, the energy was scanned from 10206 to 10156 eV. For in situ single crystal XRD experiment, a ∼80 × 100 μm^2 single crystal was loaded in symmetrical DAC with high purity silicone oil as the pressure-transmitting medium. The data were collected on a Bruker D8 VENTURE PHOTON II system equipped with a Microfocus Incoatec Ims 3.0 (Mo K_α, λ = 0.71073 Å). APEX 3 software (Bruker) was used to refine the collected data. The in situ high-pressure synchrotron XRD data were collected at the 5A-MS-XRS beamline of the Pohang Accelerator Laboratory. Well ground 1:1 co-crystal of AB−FAB was loaded in symmetrical DAC without the pressure-transmitting medium. The instrument was calibrated by a CeO_2 standard sample and the wavelength of incident monochromatic X-ray is 0.69265 Å. The Dioptas program was used for reducing the collected data.[45]

Synthesis of Sample (PE-20) Recovered from 20 GPa by Paris-Edinburgh Press. The sample PE-20 was synthesized by a VX3 Paris-Edinburgh (PE) press with double-toroidal sintered diamond anvils and automatic hydraulic oil syringe pump was used to drive the system. The volume of the powder sample is 31.1 mm^3. The target pressure is 1650 bar (oil pressure), about 20 GPa according to the Edinburgh group calibration curve.[46] The rate of the compression is 4 bar/min below 600 bar, 2 bar/min from 600 to 1000 bar, 1 bar/min from 1000 to 1300 bar, and 0.5 bar/min from 1300 to 1650 bar. The pressure was maintained for 1 h every 100 bar when the pressure exceeded 1000 bar. The sample was maintained at the 1650 bar for about 12 h and then decompressed to ambient pressure. The rate of decompression is the same with that in the compression process. The obtained recovered product PE-20 was used for X-ray Raman experiments.

Synthesis of Sample Recovered from 25 GPa by DAC and Its Gas Chromatography Mass Spectrometry Measurements. Powder sample AB−FAB co-crystal was loaded in DAC and compressed up to 25 GPa. After holding 2 h at 25 GPa, the sample was decompressed to ambient pressure. The AB−FAB recovered from 16 and 20 GPa were synthesized according to the same procedures described above. The recovered sample was picked out with a tungsten needle and dissolved in 10 μL of dichloromethane (CH_2Cl_2, HPLC purity, 99.9%). High-resolution gas chromatography mass spectrometry (GC−MS) of the recovered sample was carried on a Thermo Scientific Q Exactive GC hybrid quadrupole-Orbitrap mass spectrometer. 1 μL of sample was injected manually at the S/SL mode. A TG-5SilMS capillary column (30 m × 0.25 mm I.D. × 0.25 μm film thickness) was used and helium (99.999%) with a constant flow rate of 1.0 mL/min was used as the carrier gas. The GC oven was increased from 40 °C (held for 2 min) to 280 °C at a rate of 5 °C/min, and the temperature of the inlet, transfer lines and ion source were set at 280 °C. The system was operated with an electron ionization (EI) source at 70 eV. Scan spectra were recorded in the range of 50−750 m/z. The Thermo Scientific Trace-Finder 4.0 software and Thermo Scientific deconvolution software were used to acquire and process the data, respectively. The percentage (%) of each product was obtained by integrating the ion peak area of each product relative to the total ion peak area.

Metadynamic Simulation and Calculation of the IR Spectra. The geometry optimization of AB−FAB under 20 GPa

https://doi.org/10.1021/acs.jpcc.3c01450
J. Phys. Chem. C 2023, 127, 8482−8492

was performed by density functional theory (DFT) calculations by using Vienna Ab-initio Simulation Package (VASP) code.[47] The local density approximation (LDA) exchange correlation functional by Ceperley and Alder, as parameterized by Perdew and Zunger (CA−PZ)[48] in the projector-augmented plane-wave projector augmented wave potentials was used. A *k*-point sampling of less than $2\pi \times 0.05$ Å^{-1} and an energy cutoff at 640 eV were used. Molecular dynamics (MD) simulation with metadynamics method[49] implemented in VASP was conducted at 300 K, with a 640 eV energy cutoff and a Γ-point only *k*-point sampling. In the MD simulations, the unit cell containing two molecules were expanded to a supercell consisted of $2a \times 2b \times 1c$ unit cells. Each meta step consisted of 500 MD steps, 0.8 fs each step. For the calculation of the IR spectra of AB−FAB, the Cambridge Sequential Total Energy Package (CASTEP) module[50] in Material Studio was used. IR spectra were then calculated for reference.[51] DFT-D3(BJ)[52] correction was used to take the non-covalent effects into consideration in VASP, while OBS correction in CASTEP.[53]

Reaction Mechanism Calculation for Metathesis Product, $C_{12}N_2H_5F_5$ (Product 7). The chemical reaction mechanism of the formation of product 7 was performed with DFT calculations as implemented in Gaussian,[54] which is based on an isolated molecular system. All the calculations were done at the B3LYP/6-311 + g(d,p)[55−57] level with subsequent frequency calculations to confirm the true minima (zero number of imaginary frequency) or transition states (TS, with the existence of only one number of imaginary frequency). Besides, intrinsic reaction coordinate (IRC) calculations were also conducted for TSs to verify the reaction mechanism involving the existence of the N_4 ring. Pressure correction could be approximated by the volume of activation according to Hoffmann.[58] Volumes of activation was worked out by Multiwfn[59] software after defining the molecular surfaces with the isosurfaces of charge density at 0.002 a.u.[60] Relative Gibbs free energy of the states at the specified conditions was worked out according to the results above.

RESULTS AND DISCUSSION

Structural Evolution under High Pressure. We investigated the structure evolution of AB−FAB under high pressure by combining the in situ single crystal and powder XRD. At ambient pressure, the phenyl and perfluorophenyl has an ordered $\pi-\pi$ stacking as expected (Figure 1a and Table S1), with the two closest intermolecular N···N distances 3.68 and 3.80 Å, respectively. Upon compression to 2.2 GPa, the lattice parameters of AB−FAB determined by using in situ single crystal XRD, shrank but maintained its shape (Table S2). For higher pressure up to 34.7 GPa, the in situ powder XRD maintained the profile with all the peaks shifting to high angle without any new peak appearing (Figure 1b), which suggests that the $\pi-\pi$ stacking were stable and only the intermolecular distance was compressed. This is also supported by the theoretical calculation, which reveals a similar structure after optimization of AB−FAB under 20 GPa (discussed later). Hence, we can conclude that the $\pi-\pi$ stacking in AB−FAB is stable under applied pressure before reaction, which is favorable for inducing the bonding between azo groups as we expected.

In Situ Raman and IR Spectra under High Pressure. To probe the variation of the local structure, in situ Raman and IR spectra of AB−FAB under applied pressure were collected up to 25 and 40 GPa, respectively, as shown in Figure 2, and the detailed peak assignments are listed in Tables S3 and S4. Upon

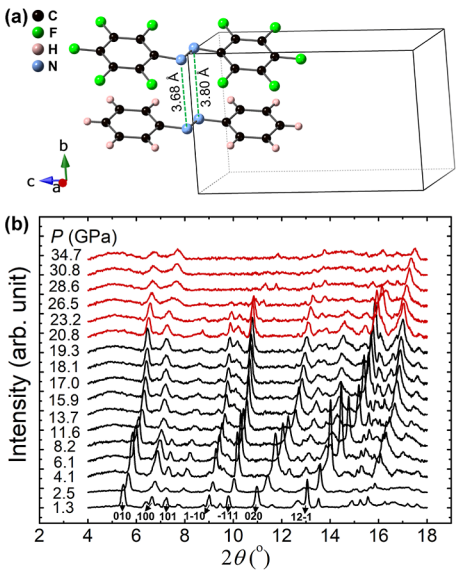

Figure 1. (a) Crystal structure of AB and FAB co-crystal [*P*-1, a = 6.1071(2) Å, b = 7.4789(2) Å, c = 11.8018(3) Å, α = 89.606(2)°, β = 85.385(2)°, and γ = 84.467(2)°]. (b) Selected XRD patterns of AB−FAB up to 34.7 GPa.

compression, all the Raman modes blue-shifted slowly (Figure 2a,b). Above 4.2 GPa, new peaks centered at 937 and 1648 cm^{-1} (marked asterisk in Figure 2a,b) emerged in the region of C−H out-plane bending and C═C stretching of azobenzene, which are probably related to the changes of the local environment of the phenyl group. Above 17.3 GPa, almost all the Raman peaks disappeared and the color of sample changed from orange to black, which indicates the chemical reaction starts. After decompression from 25.6 GPa, only a broad peak centered at 1600 cm^{-1} survived and hence demonstrated that the reaction is irreversible.

In situ IR spectra uncovered the similar transition and chemical reaction (Figure 2c,d). As displayed in Figures 2c and S1, a new peak emerged in the region of C−H out-plane bending of azobenzene (721 cm^{-1}) at 5.4 GPa, indicative of the minor transition related to the changes of the local environment of the phenyl group, consistent with the Raman results. Above 20.3 GPa, new peaks at 937 (C−H in-plane bending) and 1208 cm^{-1} appeared and gradually enhanced with the increase in pressure (asterisked in Figures 2c and S1). To confirm the new peak at 1208 cm^{-1}, we compared the in situ IR spectra of ^{14}N−AB−^{14}N−FAB co-crystal and ^{15}N−AB−^{14}N−FAB co-crystal. Both these two powder samples were placed into one DAC symmetrically to avoid the measurement error of the pressures in different sequences. At 22.4 GPa, comparing with the peak in the unlabeled sample (1212 cm^{-1}), that in the ^{15}N-labeled sample red-shifts by 12 cm^{-1} due to the isotope substitution (Figure 2e), which indicates that the new peak is related to the N atom and can be assigned to N−N or C−N stretching. This indicates that the N═N reacts to form N−N or C−N. A sp^3 C−H stretching peak also developed (red circle in Figure 2d) and became more obvious during decompression (Figure S2), which obviously resulted from the C−C bonding between the aromatic rings. Above 25.6 GPa, the IR peaks of AB−FAB gradually disappeared. Only the new bands centered at 1030, 1200, and 3210 cm^{-1} maintained up to 40 GPa and during the decompression process (Figure S2), demonstrating that the chemical reaction is irreversible. In the recovered product, the

https://doi.org/10.1021/acs.jpcc.3c01450
J. Phys. Chem. C 2023, 127, 8482−8492

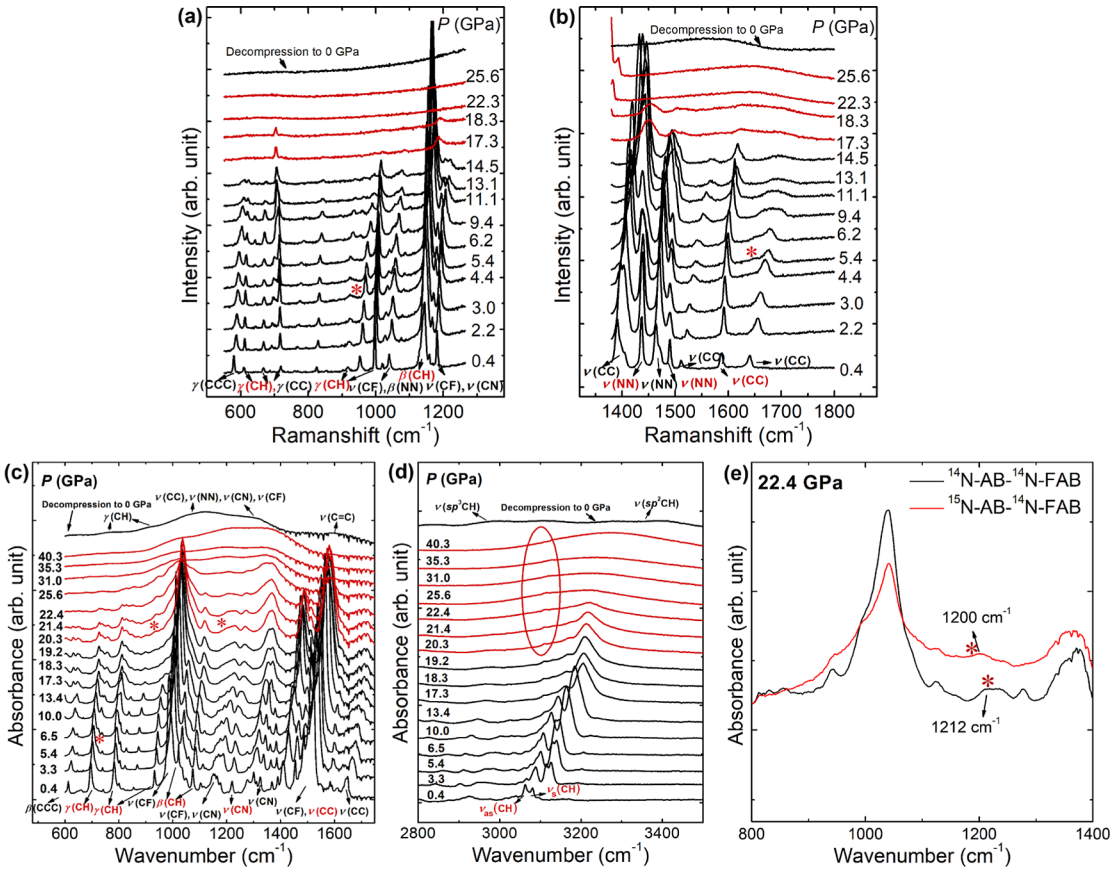

Figure 2. In situ Raman spectra of AB−FAB up to 25.6 GPa and that recovered to ambient pressure in the region of (a) 550−1280 and (b) 1380−1800 cm^{-1}. In situ IR spectra of AB−FAB up to 40.3 GPa in the region of (c) 600−1750 and (d) 2800−3500 cm^{-1}. (e) IR spectra of ^{14}N−AB−^{14}N−FAB and ^{15}N−AB−^{14}N−FAB at 22.4 GPa. γ represents out-of-plane bending; ν represents stretching; β stands for in-plane bending. The vibrations marked in black and red at 0.4 GPa belong to the FAB and AB moieties, respectively.

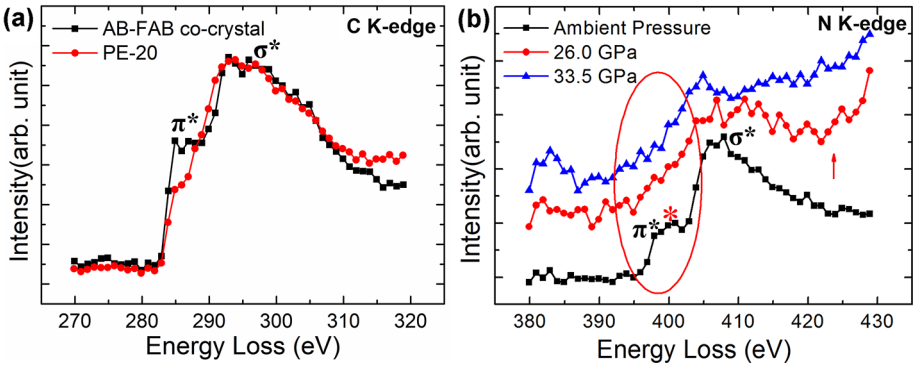

Figure 3. (a) Carbon K-edge spectra of AB−FAB and PE-20 at ambient pressure. (b) In situ nitrogen K-edge spectra of co-crystal AB−FAB under high pressure. The peak at 400 eV attributed to K → π^* transition of nitrogen marked by the asterisks decreased compared with that at ambient pressure.

two broad peaks centered at 1120 and 1310 cm^{-1} are ascribed to the C−F/C−C/C−N/N−N stretching bonded with sp^3−C and double bonds, respectively, and the sp^3 C−H stretching (2995 cm^{-1}) was also present in the product, which means that the aromatic rings experienced an irreversible bonding process in the PIP.

X-ray Raman Spectroscopy under High Pressure. X-ray Raman spectroscopy (XRS) provided elemental specific evidences on the reaction of the π-bonds of carbon and nitrogen in AB−FAB under both in situ and ex situ conditions. The carbon K-edge XRS spectra of AB−FAB co-crystal and the product synthesized by PE press at 20 GPa (referred as PE-20) are shown in Figure 3a. The K → π^* transition band of carbon (~285 eV) in PE-20 obviously decreases, which indicates part of C−C π bonds transformed to σ bonds irreversibly. This agrees with the appearance of sp^3 C−H in IR results, and hence confirms that the phenyl involved in the reaction to form the sp^3 C. On the other hand, the in situ experiment shows that the signal of K → π^* transition of nitrogen (at 400 eV, asterisked in Figure 3b) also significantly decreases under high pressure, while the K → σ^* transition band obviously increases above 415 eV. This clearly suggests that the N═N π-bond takes part in the reaction and converts into the σ bond.

https://doi.org/10.1021/acs.jpcc.3c01450
J. Phys. Chem. C 2023, 127, 8482−8492

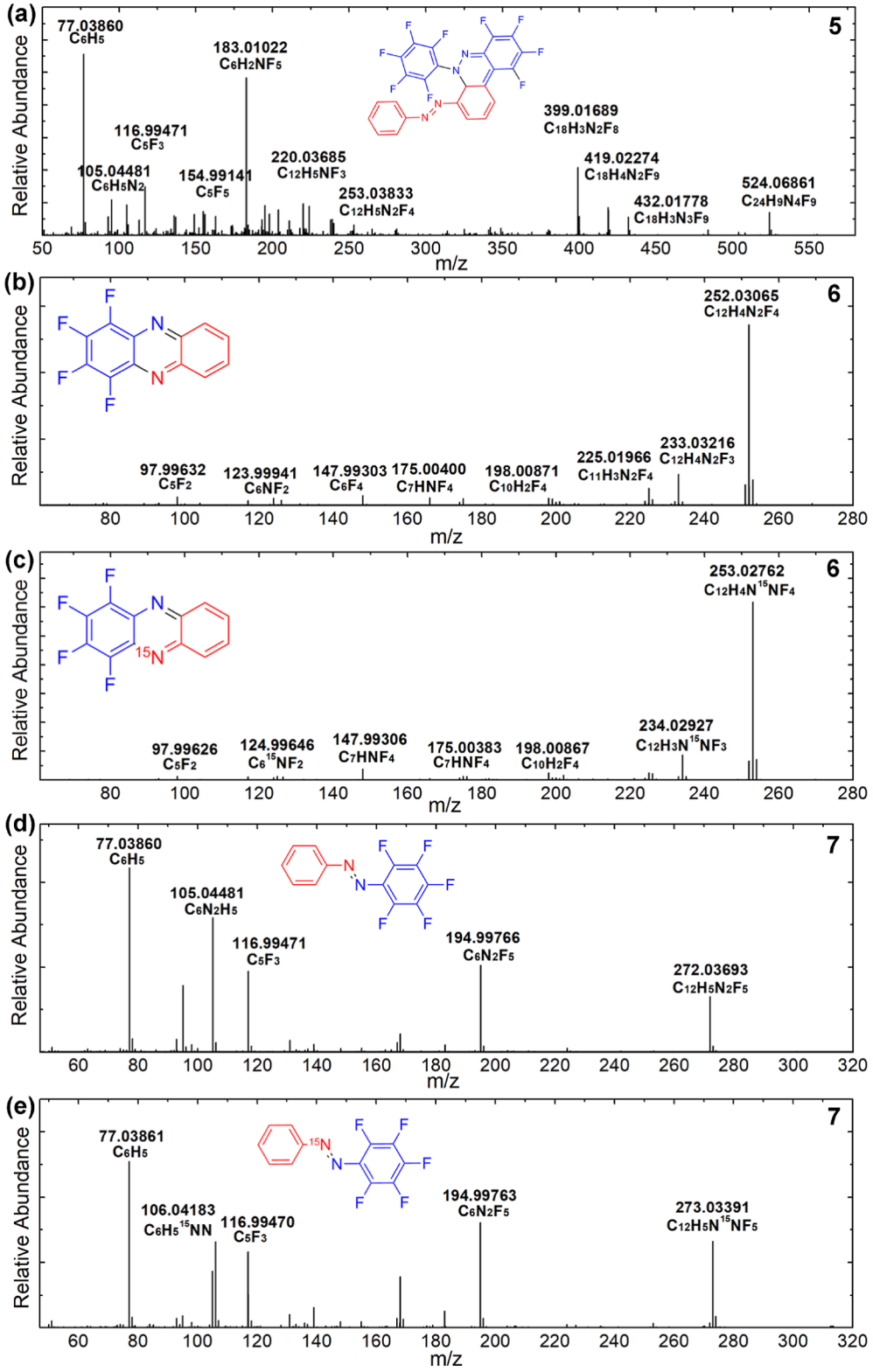

Figure 4. GC−MS on the recovered product from 25 GPa. (a) $C_{24}N_4H_9F_9$, (b) 1,2,3,4-tetrafluorophenazine, (c) isotope-labeled 1,2,3,4-tetrafluorophenazine $C_{12}H_4{}^{15}NNF_4$, (d) metathesis product 1-(perfluorophenyl)-2-phenyldiazene $C_6H_5{-}N{=}N{-}C_6F_5$, and (e) isotope-labeled product $C_6H_5{-}{}^{15}N{=}N{-}C_6F_5$.

Gas Chromatography Mass Spectrometry of Recovered Products. In order to understand the reaction process, we performed the GC−MS to investigate the structure of the intermediate products. The sample recovered from 25 GPa in DAC experiments was extracted by dichloromethane (CH_2Cl_2) and the soluble oligomers/intermediates were investigated by the GC−MS. The total ion chromatograms (TIC) of the products of AB−FAB recovered from 25 GPa are displayed in Figure S3 and seven primary compounds were detected (marked **1**−**7** in Figures S3 and S4a), including $C_6F_5NH_2$ (**1**,

https://doi.org/10.1021/acs.jpcc.3c01450
J. Phys. Chem. C 2023, 127, 8482−8492

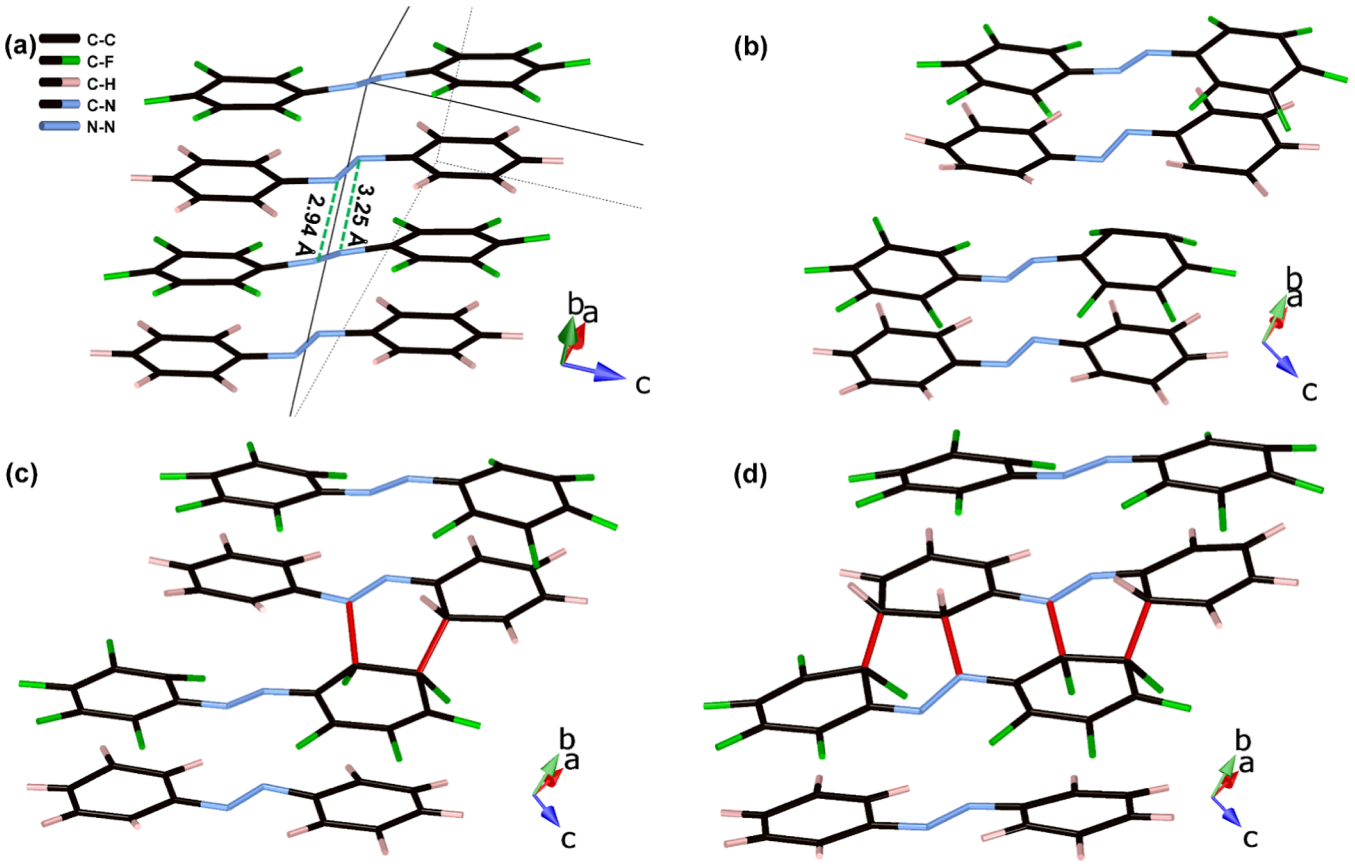

Figure 5. (a) Crystal structure of AB−FAB under 20 GPa after geometry optimization. The 23rd step of metadynamic simulation: (b) before reaction, (c) 0.8 and (d) 40.8 fs later. Red bonds are the newly formed bonds.

pentafluoroaniline, 38%), H−F-exchanged product C_6F_5−N═N−C_6F_4H (**2**, 24%), C_6H_5−N═N−C_6H_4F (**3**, 2%), nitrogen-loss exchanged product C_6F_5−NH−C_6H_5 (**4**, 11%), dimmer $C_{24}N_4H_9F_9$ (**5**, 8%), exchanged products $C_{12}N_2H_4F_4$ (**6**, 3%), and to our surprise, metathesis product, $C_{12}N_2H_5F_5$ (**7**, 7%).

4 is identified as 2,3,4,5,6-pentafluoro-*N*-phenylaniline (Figure S5). Checking the GC−MS results of the recovered high-pressure product (25 GPa) of isotope-labeled ^{15}N−AB−^{14}N−FAB co-crystal (Figure S4b), the N atom is from FAB. It proves that the C atom of AB bonds to the N of FAB under high pressure. **5** is a dimmer with one H and one F atom eliminated and is determined as (*E*)-7,8,9,10-tetrafluoro-5-(perfluorophenyl)-4-(phenyldiazenyl)-4a,5-dihydrobenzo[*c*]-cinnoline (Figure 4a). The molecular structure was determined by the tandem mass spectrometry (MS/MS) of the selected ions $C_{24}H_9N_4F_9$, $C_{18}H_4N_2F_9$, and $C_{18}H_3N_2F_8$ (Figure S6). This product is from the Diels−Alder reaction between −N═N−CF═CF− of FAB and −CH═CH− in AB, which was confirmed again by the meta-dynamic calculation results of AB−FAB discussed below. **6** is identified as the 1,2,3,4-tetrafluorophenazine (Figure 4b) by comparing the MS with phenazine, perfluorophenazine, and benzo[*c*]cinnoline (Figure S7). The two nitrogen atoms are from AB and FAB, respectively, as demonstrated by the isotope-labeled experiment (Figure 4c). It also evidences the intermolecular bonding between C and N under high pressure.

7 is identified as 1-(perfluorophenyl)-2-phenyldiazene (Figure 4d) due to its similar fragmentation process with AB and FAB (Figure S8). The isotope-labeled experiment identified C_6H_5−^{15}N═N−C_6F_5 from the product (Figure 4e), and therefore unambiguously demonstrated that the two nitrogen atoms in the metathesis product are from ^{15}N labeled AB (C_6H_5−^{15}N═^{15}N−C_6H_5) and non-labeled FAB (C_6F_5−N═N−C_6F_5), respectively, via a direct N−^{15}N bonding under high pressure. It should be noted that **7** differs from **4**−**6** by new N−N bonding, which should result from completely different reaction paths.

Metadynamic Calculation. To understand the bonding process, we optimized the crystal structure at 20 GPa by theoretical calculation (Figure 5a). The stacking between the phenyl and perfluorophenyl units resembles that at ambient pressure, in consistence with the XRD data. The closest intermolecular N···N distances are 3.25 and 2.94 Å, respectively. Starting from this model we performed metadynamic calculation to simulate the reaction routes. At the 23rd step, the [4 + 2] Diels−Alder reaction between the phenyl-ring of FAB (−CF═CF−) and the phenyl-azo group of AB (−CH═CH−N═N−) takes place (Figure 5b,c). The time interval between the formation of the two new bonds is less than 0.8 fs and hence demonstrated the concerned reaction. The same reaction also happens between the phenyl-ring of AB (−CH═CH−) and phenyl-azo group of FAB (−CF═CF−N═N−) after 40.8 fs (Figure 5d). A dimer containing seven fused rings is thus formed, as shown in Figure 5d. As the reaction continues, a layered polymeric network was formed (Figure S9). Part of the sp^2 C of phenyl and perfluorophenyl moieties transferred into sp^3 C, in agreement with the spectroscopic and XRS results. This structure maintains in the following optimization at ambient pressure.

https://doi.org/10.1021/acs.jpcc.3c01450
J. Phys. Chem. C 2023, 127, 8482−8492

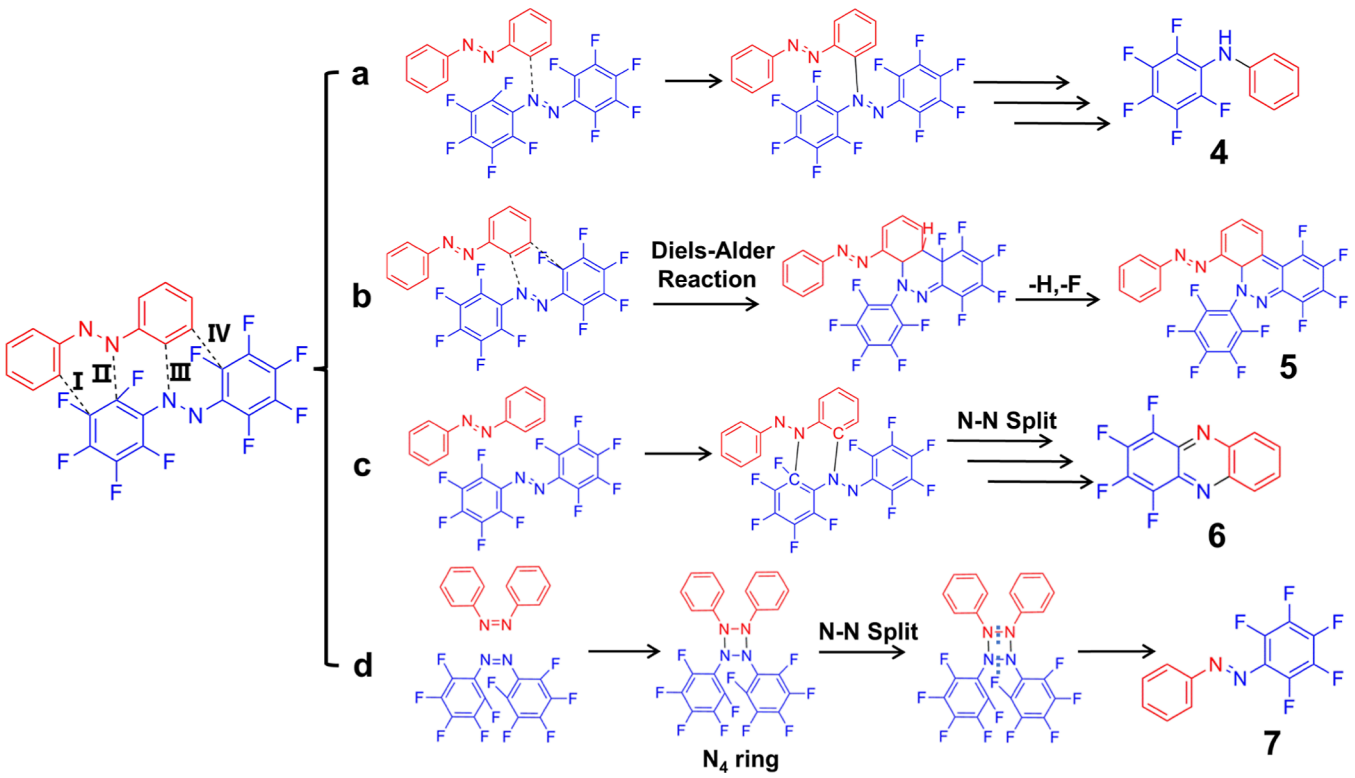

Figure 6. Reaction route for forming (a) 2,3,4,5,6-pentafluoro-*N*-phenylaniline, (b) dimer ($C_{24}N_4H_9F_9$), (c) 1,2,3,4-tetrafluorophenazine, and (d) 1-(perfluorophenyl)-2-phenyldiazene.

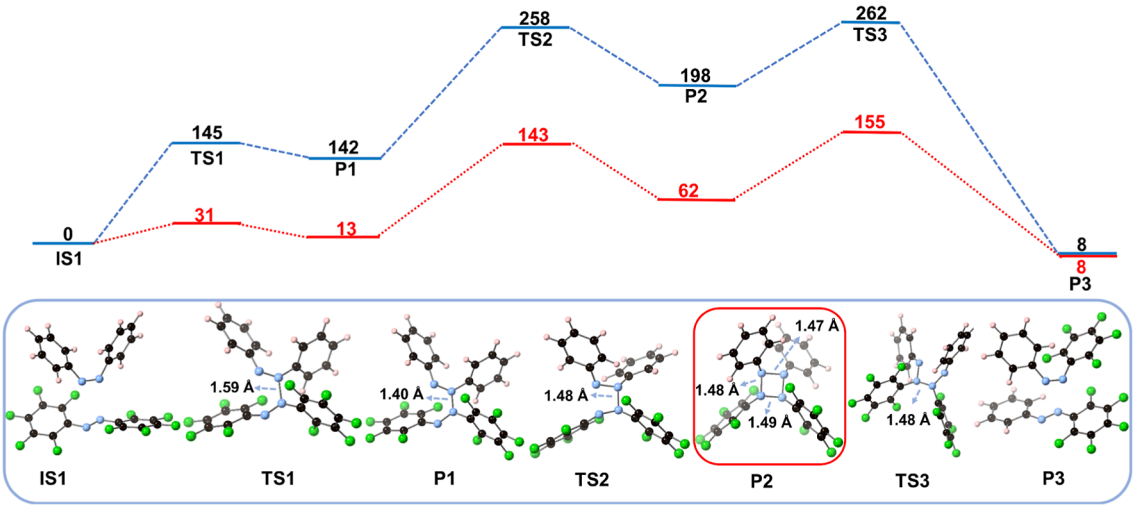

Figure 7. Gibbs free energy profile of reaction paths of the N_4 ring. Red lines represent the potential energy profile corrected by $P\Delta V^{\neq}$ and $P\Delta V$ referred to the volume of IS1. IS: initial state, TS: transition state, and P: product. The unit of energy is kJ/mol.

According to the above experimental results and meta-dynamic simulation, four possible bonding (I, II, III, and IV) between AB and FAB are suggested as shown in Figure 6, which explained the formation of the products **4**–**6** observed in GC–MS by new C–N and C–C bonds. The bonding is obviously topochemical. **4** is generated from the bonding III (path a) and following elimination of N–C_6F_5 and N_2–C_6H_5. By bonding of III and IV, **5** is generated from the Diels–Alder reaction between −N═N−CF═CF− of FAB and −CH═CH− in AB (path b). In this route, phenyl is dienophile and pentafluorophenyldiazenyl is diene, as found in the meta-dynamic results. **6** is generated via the bonding of II and III (path c) and the breaking of N–N bond, which is in fact a [3 + 3] cycloaddition[61] between N−CF═CF− of FAB and −CH═CH−N in AB.

Reaction Mechanism Calculation. The formation of 7 with the new N–N bond should follow another route. An intermediate product containing the N_4 ring, 1,2-bis-(perfluorophenyl)-3,4-diphenyltetrazetidine, is proposed via [2 + 2] cycloaddition of two azo groups. It will decompose by N–N splitting during decompression, and forming 7, as evidenced by the GC–MS experiment. The corresponding chemical reaction mechanism was investigated by DFT calculation, and three TSs and intermediates were found at ambient pressure, as shown by the blue line in Figure 7. The Cartesian coordinates of each

https://doi.org/10.1021/acs.jpcc.3c01450
J. Phys. Chem. C 2023, 127, 8482−8492

structure are shown in Tables S5−S11. At ambient pressure, AB and FAB first experienced TS1 with energy barrier of 145 kJ/mol and formed P1 with the two molecules linked by one N−N bond. Then, P1 changed conformation via TS2 with an energy barrier of 116 kJ/mol, followed by the formation of the second N−N bond, releasing 60 kJ/mol of energy to form a N_4 ring (P2). The bond lengths of N−N are ∼1.48 Å, which was closed to the N−N single bond lengths in hydrazine (1.452 Å).[62] The bond angles of N_4 ring are ∼90°, suggesting that the N_4 ring has a planar configuration. The energy difference between IS1 and P2 is 198 kJ/mol, which is similar with the energy difference between two N═N bonds and four N−N bonds at ambient pressure, 168 kJ/mol. The N_4 ring of P2 easily decomposes via TS3 (with the energy barrier of only 64 kJ/mol) and form **7**, which is detected in GC−MS of high-pressure products.

To investigate the formation mechanism of **7** under high pressure, we included the contribution of the PV term to enthalpy according to Hoffmann's report,[58] where the volume of activation ($\Delta V^{\neq} = V_{\text{transition state}} - V_{\text{initial state}}$) and the volume change for reaction ($\Delta V = V_{\text{final state}} - V_{\text{initial state}}$) significantly affect the reaction. The values of $\Delta V^{\neq}$ and ΔV referred to the volume of initial state (IS1) for all the species in the reaction profiles were obtained by Multiwfn[59] software at 0 GPa, with defining the molecular surfaces at the isosurfaces of charge density at 0.002 a.u (Table 1).[60] When pressure goes up to 20 GPa, the enthalpy changes, $\Delta H^{\neq} = U^{\neq} + P\Delta V^{\neq}$ and $\Delta H = U + P\Delta V$, are corrected by $P\Delta V^{\neq}$ and $P\Delta V$ for TSs and intermediates, respectively, and the overall energy profile is shown in Figure 7 (red lines) with the details shown in Table S12. For P1 and P2, the relative Gibbs free energy will decrease by 129 and 136 kJ/mol, respectively. P1 is hence located in a shallow potential well with an energy barrier of 31 kJ/mol (only 18 kJ/mol to TS1), reversible between IS1 and P1. P2 is only 62 kJ/mol above IS1, which means thermodynamically the N_4 ring is an accessible intermediate product under 20 GPa and room temperature. The relative Gibbs free energy of TS1 and TS2 also decreases to 31 and 143 kJ/mol as corrected by $P\Delta V^{\neq}$, respectively. Thus, only the second transition determines the formation of the N_4 ring. This is a high energy barrier but has already suppressed by external pressure significantly because forming N_4 ring is a cyclization with both negative $\Delta V^{\neq}$ and ΔV, and is accessible at room temperature and high pressure. Furthermore, the barriers of the N_4 ring going reversibly to P1 or further to P3 are 81 and 93 kJ/mol, respectively, implying its possible existence as an intermediate. Thus, we conclude the formation of the N_4 ring structure under high pressure in this system via path d in Figure 6, which formed **7** as detected in GC−MS of high-pressure products.

Table 1. Pressure−Volume Effect on the Reaction Path of Forming N_4-Ring

	TS1	P1	TS2	P2	TS3	P3
$\Delta V^{\neq}$ (Å^3)	−9.4		−9.6		−8.9	
ΔV (Å^3)		−10.7		−11.3		0.1
$P\Delta V^{\neq}$, $P\Delta V$ (kJ/mol)	−114	−129	−115	−136	−107	0

The reaction path of azo groups under high pressure is diversified but quite different with that in ambient pressure. At ambient pressure, due to the strong electron-withdrawing ability of the azo group, azo groups were reported as dienophiles to react with diene in the hetero-Diels−Alder reaction in last decades.[63−67] In contrast, under high pressure, the regular molecular stacking and the spatial selectivity of high-pressure solid reaction determines that the azo groups participate in the hetero-Diels−Alder reaction as a part of dienes and even the phenyl groups can also participate in the reactions. Besides, due to the strong stacking restriction caused by applying pressure, the distance between adjacent azo groups could be close enough and the [2 + 2] reaction could also occur to form the N_4 ring. In the decomposition process, due to the thermal instability of the four-membered ring, the metathesis products are observed, which played key evidence of the formation of four-membered ring.[32,68] We also found that the content of metathesis product increased upon further compression. The content ratio of product **7** to (**4** + **5** + **6**) was 17% at 20 GPa, and 32% at 25 GPa, which indicates these two reactions are competitive and high pressure facilitates the formation of the N_4 ring system.

CONCLUSIONS

To conclude, by employing the $\pi\cdots\pi$ intermolecular interaction between benzene and hexafluorobenzene, the co-crystal of azobenzene and perfluoroazobenzene was constructed and its reaction under high pressure up to 40 GPa was studied. The spectroscopic, XRD, XRS, GC−MS, and theoretical investigations evidence two kinds of reactions: the [4 + 2] Diels−Alder reaction between the azo and phenyl group and the [2 + 2] reaction between the azo groups happen under high pressure. The resulted N_4 (tetrazetidine) ring is not stable and transfers into the metathesis product C_6H_5−N═N−C_6F_5, which is observed in GC−MS and confirmed solidly by the isotope-labeled experiment and theoretical calculation. This is the first time to experimentally observe the metathesis product of azo, and through this, the presence of the N_4 intermediate is evidenced. The parallel arene-perfluoroarene π-stacking arrangement and high pressure are responsible for the [2 + 2] bonding between the azo groups. Our studies show that the extreme condition combining the crystal engineering is an effective way to synthesize poly-nitrogen compounds.

ASSOCIATED CONTENT

Supporting Information

The Supporting Information is available free of charge at https://pubs.acs.org/doi/10.1021/acs.jpcc.3c01450.

Experimental procedures, IR spectra, TIC of the products, contents of recovered products, mass spectra comparison, tandem mass spectrometry, metadynamic simulation, nuclear magnetic resonance of raw materials, atomic coordinates of AB−FAB at ambient pressure, lattice parameters of AB−FAB under high pressure, assignments of Raman and IR modes of the AB−FAB co-crystal, Cartesian coordinates, and energy corrections in the reaction mechanism (PDF)

AUTHOR INFORMATION

Corresponding Authors

Haiyan Zheng − *Center for High Pressure Science and Technology Advanced Research, Beijing 100193, P. R. China;* orcid.org/0000-0002-4727-5912; Email: zhenghy@hpstar.ac.cn

Le Kang − *Institute of High Energy Physics, Chinese Academy of Sciences, Beijing 100049, P. R. China; Spallation Neutron Source Science Center, Dongguan 523803, P. R. China;* Email: kangl@ihep.ac.cn

https://doi.org/10.1021/acs.jpcc.3c01450
J. Phys. Chem. C 2023, 127, 8482−8492

Authors

Dexiang Gao − *Institute of High Energy Physics, Chinese Academy of Sciences, Beijing 100049, P. R. China; Spallation Neutron Source Science Center, Dongguan 523803, P. R. China; Center for High Pressure Science and Technology Advanced Research, Beijing 100193, P. R. China*

Xingyu Tang − *Center for High Pressure Science and Technology Advanced Research, Beijing 100193, P. R. China*

Chunfang Zhang − *College of Chemistry and Materials Science, Hebei University, Baoding 071002, P. R. China;* orcid.org/0000-0003-0768-0531

Yajie Wang − *Center for High Pressure Science and Technology Advanced Research, Beijing 100193, P. R. China*

Xin Yang − *Center for High Pressure Science and Technology Advanced Research, Beijing 100193, P. R. China*

Peijie Zhang − *Center for High Pressure Science and Technology Advanced Research, Beijing 100193, P. R. China;* orcid.org/0000-0001-6355-5482

Xuan Wang − *Center for High Pressure Science and Technology Advanced Research, Beijing 100193, P. R. China;* orcid.org/0000-0001-6647-9542

Jingqin Xu − *Center for High Pressure Science and Technology Advanced Research, Beijing 100193, P. R. China*

Jie Su − *College of Chemistry and Molecular Engineering, Peking University, Beijing 100871, P. R. China;* orcid.org/0000-0001-9800-3370

Fuyang Liu − *Center for High Pressure Science and Technology Advanced Research, Beijing 100193, P. R. China*

Xiao Dong − *Key Laboratory of Weak-Light Nonlinear Photonics, School of Physics, Nankai University, Tianjin 300071, P. R. China;* orcid.org/0000-0003-4533-1914

Xiaohuan Lin − *Center for High Pressure Science and Technology Advanced Research, Beijing 100193, P. R. China*

Bao Yuan − *Institute of High Energy Physics, Chinese Academy of Sciences, Beijing 100049, P. R. China; Spallation Neutron Source Science Center, Dongguan 523803, P. R. China*

Nozomu Hiraoka − *National Synchrotron Radiation Research Center, Hsinchu 30076, Taiwan*

Kuo Li − *Center for High Pressure Science and Technology Advanced Research, Beijing 100193, P. R. China;* orcid.org/0000-0002-4859-6099

Ho-kwang Mao − *Center for High Pressure Science and Technology Advanced Research, Beijing 100193, P. R. China*

Complete contact information is available at: https://pubs.acs.org/10.1021/acs.jpcc.3c01450

Author Contributions

○D.G. and X.T. contributed equally to this paper. All authors have given approval to the final version of the manuscript.

Notes

The authors declare no competing financial interest.

■ ACKNOWLEDGMENTS

This work was supported by the National Natural Science Foundation of China (NSFC) (grant nos.: 22022101, 21875006, and 21771011). The authors also acknowledge the support of the National Key Research and Development Program of China (2019YFA0708502). Part of the calculation work was supported by the National Natural Science Foundation of China (11704024) and the Natural Science Foundation of Hebei Province (B2020201006). X.D. thanks the support of the Nature Science Foundation of Tianjin (grant no. 20JCYBJC01530). B.Y. acknowledges the Youth Innovation Promotion Association CAS. In situ high pressure angle-dispersive X-ray diffraction experiments were performed at the 5A-MS-XRS beamline facility of the Pohang Accelerator Laboratory, BL10XU of Spring-8 and 15U1 beamline of Shanghai Synchrotron Radiation Facility (SSRF). In situ high pressure Inelastic X-ray Raman spectrum was collected on BL12XU of Spring-8. The authors thank Dr. Hyun Hwi Lee for supporting the in situ X-ray diffraction measurements under high pressure.

■ REFERENCES

(1) Kildahl, N. K. Bond Energy Data Summarized. *J. Chem. Educ.* **1995**, *72*, 423−424.

(2) Cacace, F.; de Petris, G.; Troiani, A. Experimental Detection of Tetranitrogen. *Science* **2002**, *295*, 480−481.

(3) Nguyen, M. T. Polynitrogen Compounds: 1. Structure and Stability of N_4 and N_5 Systems. *Coord. Chem. Rev.* **2003**, *244*, 93−113.

(4) Glukhovtsev, M. N.; Von Ragué Schleyer, P. The N_4 Molecule has an Open-Chain Triplet C_{2h} Structure. *Int. J. Quantum Chem.* **1993**, *46*, 119−125.

(5) Francl, M. M.; Chesick, J. P. The N_4 Molecule and Its Metastability. *J. Phys. Chem.* **1990**, *94*, 526−528.

(6) Korkin, A. A.; Balkova, A.; Bartlett, R. J.; Boyd, R. J.; Schleyer, P. V. R. The 28-Electron Tetraatomic Molecules: N_4, CN_2O, BFN_2, C_2O_2, B_2F_2, CBFO, C_2FN, and BNO_2. Challenges for Computational and Experimental Chemistry. *J. Phys. Chem.* **1996**, *100*, 5702−5714.

(7) Venanzi, T. J.; Schulman, J. M. The N_4 Molecule and the N_3^+ Ion. *Mol. Phys.* **1975**, *30*, 281−287.

(8) Glukhovtsev, M. N.; Laiter, S. Thermochemistry of Tetrazete and Tetraazatetrahedrane: A High-Level Computational Study. *J. Phys. Chem.* **1996**, *100*, 1569−1577.

(9) Wang, P.; Lin, Q.; Xu, Y.; Lu, M. Pentazole Anion Cyclo-N_5^-: A Rising Star in Nitrogen Chemistry and Energetic Materials. *Sci. China: Chem.* **2018**, *61*, 1355−1358.

(10) Christe, K. O. Recent Advances in the Chemistry of N_5^+, N_5^- and High-Oxygen Compounds. *Explos. Pyrotech.* **2007**, *32*, 194−204.

(11) Choi, C.; Yoo, H. W.; Goh, E. M.; Cho, S. G.; Jung, Y. $Ti(N_5)_4$ as a Potential Nitrogen-Rich Stable High-Energy Density Material. *J. Phys. Chem. A* **2016**, *120*, 4249−4255.

(12) Dixon, D. A.; Feller, D.; Christe, K. O.; Wilson, W. W.; Vij, A.; Vij, V.; Jenkins, H. D. B.; Olson, R. M.; Gordon, M. S. Enthalpies of Formation of Gas-Phase N_3, N_3^-, N_5^+, and N_5^- from Ab Initio Molecular Orbital Theory, Stability Predictions for $N_5^+N_3^-$ and $N_5^+N_5^-$, and Experimental Evidence for the Instability of $N_5^+N_3^-$. *J. Am. Chem. Soc.* **2004**, *126*, 834−843.

(13) Raczynska, E. D. On the Basicity and π-Electron Delocalization of 'Hexaazabenzene' N_6-Quantum-Chemical Studies. *Comput. Theor. Chem.* **2011**, *971*, 38−41.

(14) Lauderdale, W. J.; Stanton, J. F.; Bartlett, R. J. Stability and Energetics of Metastable Molecules: Tetraazatetrahedrane (N_4), Hexaazabenzene (N_6), and Octaazacubane (N_8). *J. Phys. Chem.* **1992**, *96*, 1173−1178.

(15) Curtius, T. Ueber Stickstoffwasserstoffsäure (Azoimid) N_3H. *Ber. Dtsch. Chem. Ges.* **1890**, *23*, 3023−3033.

(16) Christe, K. O.; Wilson, W. W.; Sheehy, J. A.; Boatz, J. A. N_5^+: A Novel Homoleptic Polynitrogen Ion as a High Energy Density Material. *Angew. Chem., Int. Ed.* **1999**, *38*, 2004−2009.

(17) Vij, A.; Wilson, W. W.; Vij, V.; Tham, F. S.; Sheehy, J. A.; Christe, K. O. Polynitrogen Chemistry. Synthesis, Characterization, and Crystal Structure of Surprisingly Stable Fluoroantimonate Salts of N_5^+. *J. Am. Chem. Soc.* **2001**, *123*, 6308−6313.

(18) Christe, K. O. Polynitrogen Chemistry Enters the Ring. *Science* **2017**, *355*, 351.

(19) Zhang, C.; Sun, C. G.; Hu, B. C.; Yu, C. M.; Lu, M. Synthesis and Characterization of the Pentazolate Anion cyclo-N_5^- in $(N_5)_6(H_3O)_3(NH_4)_4Cl$. *Science* **2017**, *355*, 374−376.

(20) Larson, A.; Larsson, M.; Ostmark, H. Theoretical Study of Rectangular (D_{2h}) N_4. *J. Chem. Soc., Faraday Trans.* **1997**, *93*, 2963−2966.
(21) Ritter, G.; Haefelinger, G.; Lueddecke, E.; Rau, H. Tetrazetidine: Ab Initio Calculations and Experimental Approach. *J. Am. Chem. Soc.* **1989**, *111*, 4627−4635.
(22) Glukhovtsev, M. N.; Bach, R. D.; Laiter, S. High-Level Computational Study on the Thermochemistry of Saturated and Unsaturated Three- and Four-Membered Nitrogen and Phosphorus Rings. *Int. J. Quantum Chem.* **1997**, *62*, 373−384.
(23) Ball, D. W. High-Level Ab Initio Calculations on Hydrogen−Nitrogen Compounds. Thermochemistry of Tetrazetidine, N_4H_4. *J. Mol. Struct.: THEOCHEM* **2002**, *619*, 37−43.
(24) Alcaide, B.; Almendros, P.; Aragoncillo, C. Exploiting [2+2] Cycloaddition Chemistry: Achievements with Allenes. *Chem. Soc. Rev.* **2010**, *39*, 783−816.
(25) Poplata, S.; Tröster, A.; Zou, Y.; Bach, T. Recent Advances in the Synthesis of Cyclobutanes by Olefin [2 + 2] Photocycloaddition Reactions. *Chem. Rev.* **2016**, *116*, 9748−9815.
(26) Robiette, R.; Marchand-Brynaert, J. *Comprehensive Organic Synthesis*, 2nd ed.; Elsevier: Oxford, 2014; Vol. 5, pp 85-122.
(27) Huang, C.; Zheng, M.; Xu, J.; Zhang, Y. Photo-Induced Cycloaddition Reactions of α-Diketones and Transformations of the Photocycloadducts. *Molecules* **2013**, *18*, 2942−2966.
(28) Guillemin, J. C.; Denis, J. M.; Lablache-Combier, A. 1-Azetine: Thermal Ring Opening to 2-Azabutadiene. *J. Am. Chem. Soc.* **1981**, *103*, 468−469.
(29) Sugie, M.; Takeo, H.; Matsumura, C. A Study of the Thermal Decomposition and Dehydrochlorination of *N*-Chloroazetidine: Microwave Spectra of *N*-Chloromethylenimine, 1-Azetine, and 2-Azabutadiene. *J. Am. Chem. Soc.* **1989**, *111*, 906−910.
(30) Hall, J. H.; Bigard, W. S. 1,2-Diazetidine Conformation. Double Nitrogen Inversion. *J. Org. Chem.* **1978**, *43*, 2785−2788.
(31) Kerber, R. C.; Porter, A. Structure of an Alleged Triazetidine. *J. Org. Chem.* **1968**, *33*, 3663−3665.
(32) Fischer, G.; Fritz, H.; Rihs, G.; Hunkler, D.; Exner, K.; Knothe, L.; Prinzbach, H. Proximate, *syn*-Periplanar, Rigid Imine (Nitrone)/Ene-and Diazene (Diazeneoxy)/Ene Systems: Syntheses, Homoconjugate Reactivity and Photochemistry. *Eur. J. Org. Chem.* **2000**, *2000*, 743−762.
(33) Exner, K.; Fischer, G.; Bahr, N.; Beckmann, E.; Lugan, M.; Yang, F.; Rihs, G.; Keller, M.; Hunkler, D.; Knothe, L.; et al. Proximate, *syn*-Periplanar Bisdiazene Skeletons: Syntheses, Structures, Homoconjugate Reactivity and Photochemistry. *Eur. J. Org. Chem.* **2000**, *2000*, 763−785.
(34) Exner, K.; Fischer, G.; Lugan, M.; Fritz, H.; Hunkler, D.; Keller, M.; Knothe, L.; Prinzbach, H. Proximate, *syn*-Periplanar Diazene/Diazene(di)oxy, Diazeneoxy/Diazene(di)oxy, and Diazenedioxy/Diazenedioxy Skeletons: Syntheses, [2+2] Photocycloadditions, Metathesis. *Eur. J. Org. Chem.* **2000**, *2000*, 787−806.
(35) Camp, D.; Campitelli, M.; Hanson, G. R.; Jenkins, I. D. Formation of an Unusual Four-Membered Nitrogen Ring (Tetrazetidine) Radical Cation. *J. Am. Chem. Soc.* **2012**, *134*, 16188−16196.
(36) Tomasino, D.; Kim, M.; Smith, J.; Yoo, C. S. Pressure-Induced Symmetry-Lowering Transition in Dense Nitrogen to Layered Polymeric Nitrogen (LP-N) with Colossal Raman Intensity. *Phys. Rev. Lett.* **2014**, *113*, 205502.
(37) Goncharov, A. F.; Gregoryanz, E.; Mao, H. K.; Liu, Z.; Hemley, R. J. Optical Evidence for a Nonmolecular Phase of Nitrogen above 150 GPa. *Phys. Rev. Lett.* **2000**, *85*, 1262−1265.
(38) Eremets, M. I.; Gavriliuk, A. G.; Trojan, I. A.; Dzivenko, D. A.; Boehler, R. Single-Bonded Cubic form of Nitrogen. *Nat. Mater.* **2004**, *3*, 558−563.
(39) Schettino, V.; Bini, R. Molecules under Extreme Conditions: Chemical Reactions at High Pressure. *Phys. Chem. Chem. Phys.* **2003**, *5*, 1951−1965.
(40) Wang, Y.; Yang, X.; Tang, X.; Wang, X.; Li, Y.; Lin, X.; Dong, X.; Yang, D.; Zheng, H.; Li, K.; et al. Pressure Gradient Squeezing Hydrogen out of MnOOH: Thermodynamics and Electrochemistry. *J. Phys. Chem. Lett.* **2021**, *12*, 10893−10898.
(41) Bléger, D.; Schwarz, J.; Brouwer, A. M.; Hecht, S. o-Fluoroazobenzenes as Readily Synthesized Photoswitches Offering Nearly Quantitative Two-Way Isomerization with Visible Light. *J. Am. Chem. Soc.* **2012**, *134*, 20597−20600.
(42) Sheldrick, G. M. SHELXT - Integrated Space-Group and Crystal-Structure Determination. *Acta Crystallogr., Sect. C: Struct. Chem.* **2015**, *71*, 3−8.
(43) Mao, H. K.; Xu, J.; Bell, P. M. Calibration of the Ruby Pressure Gauge to 800 kbar under Quasi-Hydrostatic Conditions. *J. Geophys. Res.* **1986**, *91*, 4673−4676.
(44) Cai, Y. Q.; Chow, P.; Chen, C. C.; Ishii, H.; Tsang, K. L.; Kao, C. C.; Liang, K. S.; Chen, C. T. Optical Design and Performance of the Taiwan Inelastic X-Ray Scattering Beamline (BL12XU) at Spring-8. *AIP Conf. Proc.* **2004**, *705*, 340−343.
(45) Prescher, C.; Prakapenka, V. B. DIOPTAS: a Program for Reduction of Two-Dimensional X-ray Diffraction Data and Data Exploration. *High Pressure Res.* **2015**, *35*, 223−230.
(46) Salmon, P. S.; Drewitt, J. W. E.; Whittaker, D. A. J.; Zeidler, A.; Wezka, K.; Bull, C. L.; Tucker, M. G.; Wilding, M. C.; Guthrie, M.; Marrocchelli, D. Density-Driven Structural Transformations in Network forming Glasses: A High-Pressure Neutron Diffraction Study of GeO_2 Glass up to 17.5 GPa. *J. Phys.: Condens. Matter* **2012**, *24*, 415102.
(47) Kresse, G.; Furthmüller, J. Efficiency of Ab-Initio Total Energy Calculations for Metals and Semiconductors Using a Plane-Wave Basis Set. *Comput. Mater. Sci.* **1996**, *6*, 15−50.
(48) Perdew, J. P.; Zunger, A. Self-Interaction Correction to Density-Functional Approximations for Many-Electron Systems. *Phys. Rev. B: Condens. Matter Mater. Phys.* **1981**, *23*, 5048−5079.
(49) Barducci, A.; Bonomi, M.; Parrinello, M. Metadynamics. *Wiley Interdiscip. Rev. Comput. Mol. Sci.* **2011**, *1*, 826−843.
(50) Clark, S. J.; Segall, M. D.; Pickard, C. J.; Hasnip, P. J.; Probert, M. I. J.; Refson, K.; Payne, M. C. First Principles Methods Using CASTEP. *Z. Kristallogr.* **2005**, *220*, 567−570.
(51) Baroni, S.; de Gironcoli, S.; Dal Corso, A.; Giannozzi, P. Phonons and Related Crystal Properties from Density-Functional Perturbation Theory. *Rev. Mod. Phys.* **2001**, *73*, 515−562.
(52) Grimme, S.; Ehrlich, S.; Goerigk, L. Effect of the Damping Function in Dispersion Corrected Density Functional Theory. *J. Comput. Chem.* **2011**, *32*, 1456−1465.
(53) Ortmann, F.; Bechstedt, F.; Schmidt, W. G. Semiempirical Van Der Waals Correction to the Density Functional Description of Solids and Molecular Structures. *Phys. Rev. B: Condens. Matter Mater. Phys.* **2006**, *73*, 205101.
(54) Frisch, M. J.; Trucks, G. W.; Schlegel, H. B.; Scuseria, G. E.; Robb, M. A.; Cheeseman, J. R.; Scalmani, G.; Barone, V.; Mennucci, B.; Petersson, G. A. et al. *Gaussian 09*, Revision B.01; Gaussian, Inc.: Wallingford, CT, 2010.
(55) Becke, A. D. Density-Functional Exchange-Energy Approximation with Correct Asymptotic Behavior. *Phys. Rev. A* **1988**, *38*, 3098−3100.
(56) Lee, C.; Yang, W.; Parr, R. G. Development of the Colle-Salvetti Correlation-Energy Formula into a Functional of the Electron Density. *Phys. Rev. B: Condens. Matter Mater. Phys.* **1988**, *37*, 785−789.
(57) Hariharan, P. C.; Pople, J. A. The Influence of Polarization Functions on Molecular Orbital Hydrogenation Energies. *Theor. Chim. Acta* **1973**, *28*, 213−222.
(58) Chen, B.; Hoffmann, R.; Cammi, R. The Effect of Pressure on Organic Reactions in Fluids-a New Theoretical Perspective. *Angew. Chem., Int. Ed.* **2017**, *56*, 11126−11142.
(59) Lu, T.; Chen, F. Multiwfn: A multifunctional wavefunction analyzer. *J. Comput. Chem.* **2012**, *33*, 580−592.
(60) Bader, R. F. W.; Carroll, M. T.; Cheeseman, J. R.; Chang, C. Properties of Atoms in Molecules: Atomic Volumes. *J. Am. Chem. Soc.* **1987**, *109*, 7968−7979.
(61) Chen, X.; Huang, S.; Li, J.; Yang, Q.; Yang, L.; Yu, F. Highly Regioselective and Chemoselective [3+3] Annulation of Enaminones

https://doi.org/10.1021/acs.jpcc.3c01450
J. Phys. Chem. C 2023, 127, 8482−8492

with *ortho*-Fluoronitrobenzenenes: Divergent Synthesis of Aposafranones and Their *N*-Oxides. *Org. Lett.* **2021**, *23*, 3032−3037.
(62) Shan, H.; Yang, Y.; James, A. J.; Sharp, P. R. Dinitrogen Bridged Gold Clusters. *Science* **1997**, *275*, 1460−1462.
(63) Weinreb, S. M.; Scola, P. M. N-Acyl Imines and Related Hetero Dienes in [4+2]-Cycloaddition Reactions. *Chem. Rev.* **1989**, *89*, 1525−1534.
(64) Liu, B.; Liu, T.; Luo, S.; Gong, L. Asymmetric Hetero-Diels−Alder Reaction of Diazenes Catalyzed by Chiral Silver Phosphate: Water Participates in the Catalysis and Stereocontrol. *Org. Lett.* **2014**, *16*, 6164−6167.
(65) Crouillebois, L.; Pantaine, L.; Marrot, J.; Coeffard, V.; Moreau, X.; Greck, C. Solvent-and Catalyst-Free Synthesis of Nitrogen-Containing Bicycles through Hemiaminal Formation/Diastereoselective Hetero-Diels-Alder Reaction with Diazenes. *J. Org. Chem.* **2015**, *80*, 595−601.
(66) Momiyama, N.; Tabuse, H.; Noda, H.; Yamanaka, M.; Fujinami, T.; Yamanishi, K.; Izumiseki, A.; Funayama, K.; Egawa, F.; Okada, S.; et al. Molecular Design of a Chiral Brønsted Acid with Two Different Acidic Sites: Regio-Diastereo-and Enantioselective Hetero-Diels-Alder Reaction of Azopyridinecarboxylate with Amidodienes Catalyzed by Chiral Carboxylic Acid-Monophosphoric Acid. *J. Am. Chem. Soc.* **2016**, *138*, 11353−11359.
(67) Kawasaki, M.; Yamamoto, H. Catalytic Enantioselective Hetero-Diels-Alder Reactions of an Azo Compound. *J. Am. Chem. Soc.* **2006**, *128*, 16482−16483.
(68) Kerber, R. C.; Ryan, T. J.; Hsu, S. D. Mechanism of Cycloaddition of Diphenylketene with Azo Compounds. *J. Org. Chem.* **1974**, *39*, 1215−1221.

https://doi.org/10.1021/acs.jpcc.3c01450
J. Phys. Chem. C 2023, 127, 8482−8492